Off the grid: breaking the raster scan paradigm in scanning probe microscopy by image reconstruction from position sensor data

Dominik Ziegler[1], Travis R Meyer[3], Rodrigo Farnham[2], Christophe Brune[4], Andrea L Bertozzi[3] and Paul D Ashby[1,5].

[1] Lawrence Berkeley National Laboratory, Molecular Foundry, 1 Cyclotron Road, 94720 Berkeley, CA USA

[2] Department of Mathematics and Statistics, California State University, Long Beach, 1250 Bellflower Blvd., Long Beach, CA, 90840-1001 USA

[3] Department of Mathematics, University of California Los Angeles, 405 Hilgard Avenue, Los Angeles, CA 90095-1555 USA

[4] Department of Mathematics and Computer Science, University of Münster, Einsteinstr. 62, D-48149 Münster, Germany

[5] Corresponding Author: pdashby@lbl.gov

Keywords: Scanning Probe Microscopy, Atomic force microscopy, Inpainting, Image Reconstruction, Spiral Scanning.

PACS: 07.79.-v (Scanning probe microscopes and components), 07.79.Lh (Atomic force microscopes), 07.05.Pj (Image processing), 07.05.Rm (Data presentation and visualization: algorithms and implementation).

Abstract

We present Sensor Inpainting, a new operation mode for scanning probe microscopy that uses advanced image processing techniques to render images based on position sensor data. Sensor Inpainting frees scanning probe microscopy from the paradigm of raster scanning, the scan waveforms do not need to fall on a grid, and the scanner is no longer required to be at a specific location at a given time for each data point. This drastically reduces the engineering effort of position control and enables the use of scan waveforms that are better suited for the high inertia nanopositioners of scanned probe microscopy. While in raster scanning, typically only trace or retrace images are used for display, in Archimedean spiral scans 100% of the data can be displayed and at least a two-fold increase in temporal or spatial resolution is achieved. In Sensor Inpainting, the sampling rate and grid size of the final generated image are independent variables. Sampling data a factor of two higher in the fast scan direction and displaying on a grid with around twice as many pixels as samples produces the best representations of the data.

1. Introduction

The entrenched paradigm for nanopositioning in Atomic Force Microscopy (AFM), Scanning Tunneling Microscopy (STM), and their many variants is a raster scan pattern. The German expressions for AFM and STM, “Rasterkraftmikroskopie” and “Rastertunnelmikroskopie” respectively, show how the raster concept is fundamentally linked to scanning probe techniques. But the idea of raster scanning predates AFM and STM. For applications like analog television, where transmission bandwidth was precious, it was economical that a single data series could create images without using X,Y position data. When AFM and STM were invented in the mid-1980s before digital signal acquisition became commonplace[1-3] raster scanning facilitated crafting 3D topographs from individual paper scan lines printed by pen plotters[4]. In the digital age, the advantage of raster scanning is that it speeds display and saves memory. By sampling at a constant rate, only a single channel needs to be recorded and each sample maps directly to a corresponding pixel in the final image. However, achieving non-distorted images requires the tip to be at a specific location at a given time with perfectly linear motion of the scanner. Unfortunately, piezoelectric nanopositioners have notoriously nonlinear displacement response and high inertia with mechanical resonances, which significantly compromises image accuracy. Specifically designed nonlinear output voltages can partially compensate the errors caused by piezo nonlinearities. Open-loop techniques frequently use second order modeling of piezo displacement and a few coupling terms to create a more linear displacement[5] (see figure 1a). The results are satisfactory for the fast scan axis but creep is not managed well causing errors in the slow scan axis and poor offset and zoom performance. For recently designed scanning probe microscopes it is more common to operate in a closed-loop configuration where X,Y positions are controlled using feedback[6,7] (see figure 1c). Unfortunately, feedback loops have significantly lower bandwidth than the position sensor signal such that accuracy is maintained only up to scan rates of a few lines per second. Feed-forward, also called adaptive scan, is a mode of operation very similar to open-loop but the piezo model used to transform the scan waveform is developed by measuring the response of the piezo with position sensors[8,9] in the fast scan direction. As an open-loop technique, feed-forward has high bandwidth performance but creep is not managed well. Combining feedback and feed-forward harnesses the advantages of each correction method but is complicated to implement[10]. The enormous engineering effort to control the piezo position has its roots in the paradigm of raster scanning. In the paradigm, the controller dictates strict position requirements based on the scan parameters. But position inaccuracies of the instrument do not influence how data are received and interpreted. This simplifies image display and the onus is on the instrument to provide accurate positioning even though piezo nanopositioners present formidable physical challenges. Another negative consequence of the raster scan paradigm beyond the unnecessary control of piezo position is that sequential scan lines moving in opposite directions are adjacent to each other. Any delay from either X,Y scanner control or the Z-feedback cause adjacent scan lines to be mismatched. Thus the convention is to discard half the data and only show trace or retrace in one image compromising spatial and temporal resolution.

While it may initially seem trivial, to relax X,Y control and passively measure position sensor data to create images is a much more elegant solution to the problem of poorly behaved piezo nanopositioners. The absence of any feedback in X,Y position results in the high bandwidth of open-loop scanning and greater accuracy than any piezo control system. More importantly, the technique frees us from the raster scan paradigm and enables the use of scan waveforms better matched to the physical limitations of piezoelectric nanopositioners and for which all scan time can be used to create images.

In chapter 2 we discuss the difficulties of raster scanning to display trace and retrace in a single image in greater detail. Chapter 3 introduces our new Sensor Inpainting technique to reconstruct images from sensor data. Chapter 4 highlights the results for a constant velocity Archimedean spiral, and chapter 5 presents conclusions.

2. Raster Scan Pattern

2.1 Open-Loop Scanning

Figure 1 illustrates the difficulties of raster scanning to generate accurate images from trace and retrace scan lines in a single image. The performance of conventional open and closed-loop configurations are compared. The schematic of an open-loop scan mode, the most basic positioning technique for scanning probe microscopy, is shown in figure 1a. The scan parameters (image size, resolution, and speed) define scan waveforms that drive

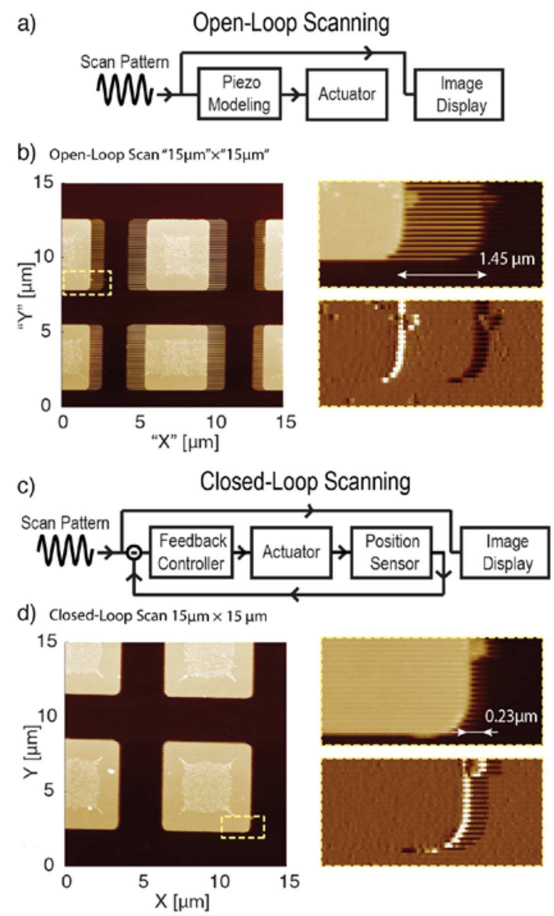

Figure 1. a) Open-loop scanning: a raster scan wave is applied in both fast and slow scan directions and they define the pixel positions for image display b) Open-loop "15 µm"x"15 µm" scan of a calibration grating using 512 scan lines (256 trace and 256 retrace). Zoom-ins of the yellow dashed rectangle region display topography and amplitude data. Piezo nonlinearity leads to 1.45 µm mismatch between trace and retrace and creep compresses the features in the slow scan direction. c) Closed-loop scanning: a feedback loop is used to control piezo position based on independent position sensor data but pixel positions are still defined by the input scan waveform. d) Closed-loop 15 µm x 15 µm scan of the same calibration grid as (b). Zoom-ins of the yellow dashed rectangle region display topography and amplitude data. The feedback controller regularizes the scan well but delay in the topography feedback loop as well as the XY position feedback cause 0.23 µm mismatch between trace and retrace.

the piezo actuator and delineate the pixel positions in the image. Figure 1b) shows topography data, where 256 trace and 256 retrace lines are displayed in the same image. All data presented in this paper were collected on a MFP-3D (Asylum Research, Santa Barbara) using amplitude modulation AFM in air with a free amplitude of 30 nm and an amplitude set-point of 24 nm. The cantilever had a nominal resonance frequency and stiffness of 70 kHz and 3 N/m respectively (Multi75Al, Budget Sensors, Bulgaria). The scan pattern was a triangular raster scan without using model based correction nor using overscan. The X,Y positions are the applied piezo voltage scaled by the first order coefficient of piezo sensitivity. The total acquisition time was 205 s, with 512 scan lines and 15 µm scan size, resulting in an average tip velocity of 37.5 µm/s. The sample features are isolated 6 µm wide squares with a spacing of 3 µm and height of 100 nm (calibration grating by Bruker Nano). The edges of the calibration steps in figure 1b) clearly show that trace and retrace scan lines do not overlay. The multi-domain structure of high sensitivity piezoelectric ceramics causes sensitivity to increase as field increases and hysteresis when field reverses such that the same applied voltage does not result in the same position. Thermally activated alignment of domains causes additional displacement or creep along the slow scan axis, such that a larger scan is compressed into the image. The zoom-ins of the yellow dashed rectangle region in figure 1 display topography and amplitude data and focus on a particle defect. This same area will be used throughout the paper for comparing all the methods discussed. Using open-loop scanning the mismatch between trace and retrace is up to 1.45 µm for a 15 µm scan or 10%. The amplitude image shows the alternating dark and light features typical for descending and climbing the step on the calibration grating. For trace and retrace they clearly do not occur at the same location. This large mismatch is mainly due to hysteresis.

2.2 Closed-Loop Scanning

Another common mode of operation is closed-loop scanning, where feedback loops control piezo position based on independent position sensor data. The pixel positions are still defined by the input scan waveform (figure 1c). Closed-loop scanning not only significantly improves image accuracy by compensating hysteresis of the piezo material (figure 1d) but also corrects for creep enabling excellent reproducibility for zooming and large offsets. Furthermore, active monitoring of the sensor allows the instrument to respond to unique mechanical characteristics of each scanner and measured drift and slip. While the large scale 15 µm x 15 µm images appear to be correct, the zoom-ins reveal a remaining discrepancy of 0.23 µm or 1.5% in the closed-loop image. Any delay from either X,Y scanner control or the Z-feedback still causes this mismatch. The result clearly demonstrates that using raster scan lines that move in opposite directions necessitates throwing away half the data for image creation, even when closed-loop operation is used.

3. Sensor Inpainting

The enormous engineering effort to control piezo position has its roots in the paradigm of raster scanning. In the paradigm, based on the scan parameters, the controller dictates strict position requirements. Sensor Inpainting relaxes this control and uses advanced image processing techniques to create gridded images from non-gridded sensor data (figure 2a). Inpainting is a class of digital image processing methods used to solve missing data problems[11]. Traditionally it has been used for such problems as digital restoration of films, artwork restoration such as old frescos[12], and removal of occlusions such as text from photographs. Special effects in the movie industry can also make use of inpainting algorithms, e.g. for removing objects/people from movies, while reasonably filling in the background[14]. Recently inpainting has also been used in 3D fluorescence microscopy or tomography to address low z-axis resolution and gaps between slices[13]. Many inpainting algorithms are based on partial differential equations[14,15,17,18] or variational minimization approaches[16]. One of the most basic inpainting methods is heat equation inpainting (also called harmonic inpainting). It has the same functional form as diffusion problems in physics and when applied to image processing it linearly diffuses the known data to unknown regions. More advanced methods better maintain edge sharpness by using total variation (TV) priors[16,20,19] representing nonlinear diffusion, or use similar regions (patch-comparisons) elsewhere in the image to inform the regions of interest (Non-Local Means, NLM)[21,22,23]. Those nonlocal and nonlinear inpainting approaches are often based on nonlocal derivatives or dictionary learning techniques[24].

In the scanning probe microscopy application, the missing data are the values of the pixels in a gridded image. The collection of these unknown, not-measured pixels is called the inpainting domain. Figure 2b) to 2e) present the steps for image generation from non-gridded data using heat equation inpainting. Figure 2b) shows the measured X,Y positions of non-gridded sensor data. The topography data recorded at each point are represented by the color of each square. To redistribute the non-gridded data back to the grid of the desired image we use linear binomial interpolation. The height information of each data point is spread to the four nearest points on the grid (figure 2c). Furthermore, we attribute to each point a weighting factor, which describes the confidence of the data,

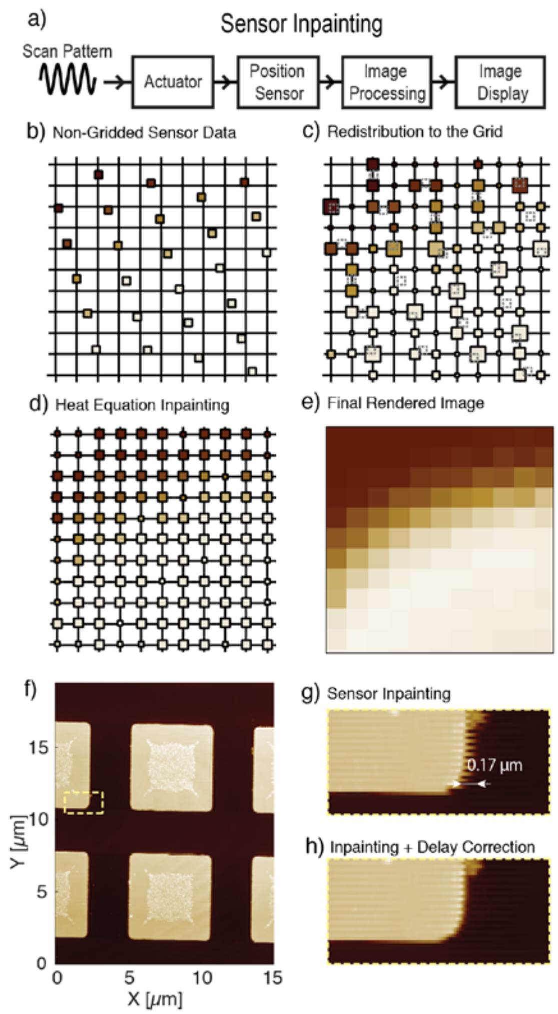

Figure 2. a) Sensor Inpainting scanning: scan waves drive the scanner and position sensor data is used to create images. b) Non-gridded position sensor data with the color of each square representing height values. c) To distribute the non-gridded data to the grid, the height information of each data point is spread to the four nearest neighbors. Close proximity of the data point to the pixel position leads to higher weights shown as size of the squares. Original data positions shown as dotted squares. d) Heat equation inpainting diffuses the existing weighted data out to the entire grid filling empty data points while denoising. e) Final rendered image f) Inpainted result from the open-loop data in figure 1b. Despite hysteresis and creep, a correct and non-distorted image is generated g) Zoom-in of dashed area in figure 2f shows good overlap of forward and backward scan lines without any control of X,Y piezo position. Mismatch is only due to Z-feedback delay. h) a delay correction can be used to improve the mismatch but subtle inaccuracies remain from raster scan lines moving in opposite directions.

and is given by the distance from the data point to the grid. When more than one data point contributes to the same pixel, the weights are used to linearly interpolate height information from the contributing data points to determine the value (figure 2c). Hence, for large data sets and coarse grids this first step might be sufficient to attribute a value to each pixel and thereby generate a full image. But pixels might remain empty when sparse data sets are projected on a fine grid. In this case, heat equation inpainting (figure 2d) diffuses the existing weighted data points over the entire grid, Ω. To this end, an energy functional,

$$\min_u E(u) = \int_\Omega |\nabla u|^2 + \int_D \lambda (u - f)^2$$

, is minimized to compute the inpainted result u (figure 2e). $D \subset \Omega$ denotes the data domain and $\Omega - D \subset \Omega$ the inpainting domain while λ is a scalar based on the weightings used to create $f: D \rightarrow R$, the weighted data points. The equation includes a gradient term to produce a smooth result and difference terms for fidelity to original measured data. Since the functional is minimized over the whole image, the relative contribution of the gradient term determines the amount of smoothing of the data during inpainting. Sensor Inpainting of open-loop data from figure 1b produces an accurate result in figure 2f. The square shape of the features and the fact that the final resulting image is elongated in the Y-axis are evidence that hysteresis and creep are accommodated properly. A full image can be restored using all the data but the zoom-ins still reveal a mismatch between trace and retrace scan lines. In the closed-loop configuration (figure 1d) the 0.23 μm discrepancy was partially due to X,Y control delay. Sensor Inpainting removes all X,Y delay however an offset of 0.17 μm remains from Z-feedback delay (figure 2g). Identifying the Z-feedback loop as a persistent source of delay between topography values and their position enables compensation of the delay by offsetting the data before generating the image using inpainting. Figure 2h shows the result with a 5 ms offset, which corrects for line mismatch. However, subtle differences between trace and retrace due to hysteresis of the Z piezo as well as effects from the z feedback loop overshooting remain. Even while using Sensor Inpainting, these unavoidable artifacts result from persisting with the raster scan paradigm. Fortunately, Sensor Inpainting enables use of scan waveforms better matched to the physical limitations of piezoelectric nanopositioners.

4. Spiral Scan Pattern

The image artifacts associated with raster scan lines moving in opposite directions necessitates throwing away half the data for image creation. Scan waves that direct the scanner to move in the same direction for adjacent scan segments enable the display of

100% of the scan data without artifacts. Scanning the perimeter of consecutively smaller concentric squares would satisfy this condition. However, stopping and starting the massive scanner is challenging, as the present need for overscan of triangular raster scan waveforms attests. As Sensor Inpainting conveniently renders non-gridded data, following a grid is not important when creating scan waveforms. Scanning a smooth spiral allows adjacent scan segments to move in the same direction and does not have sharp turns with high acceleration making it preferable for high inertia scanners. Spiral techniques are common to many data storage techniques on spinning mediums (vinyl records, hard drives, compact disks, or DVDs). But the spiral scan concept only recently found appearance in scanning profilometers[12,13], nanoscale data storage[14] or scanning probe microscopy, where spiral[15-17], cycloid[18], Lissajous[19], and various other non raster scan patterns[20] have been demonstrated. Most of these non-raster scan attempts use sensors to steer the probe over the sample in closed-loop. Spiral scanning has been shown to be useful for fast scanning[15-17]. The narrow frequency spectrum of sinusoidal scan trajectories has been shown to require less bandwidth of the feedback loop[19]. As Sensor Inpainting uses no feedback at all, its bandwidth is simply given by the performance of the position sensor itself.

In figure 3 we show the results for a constant velocity Archimedean spiral which has the simple waveform, $X = \alpha\sqrt{t}\sin\left(\beta\sqrt{t}\right)$ and $X = \alpha\sqrt{t}\cos\left(\beta\sqrt{t}\right)$, where the frequency decreases as $1/\sqrt{t}$ while the amplitude increases as $\sqrt{t}$. α and β are coefficients derived from the scan parameters: number of loops, scan size, and scan speed. Topography and amplitude data for the Sensor Inpainting results of a 256 loop spiral are shown in figure 3a and 3b respectively. For illustrating the scan direction a spiral scan pattern with few loops is overlaid onto the amplitude image. The scanned area is approximately equal to the previous 15 µm x 15 µm raster scans so 256 loops results in a similar tip velocity (37.5 µm/s) and spacing between adjacent scan lines as used in figures 1b and 2f. Sensor Inpainting diffuses data to the edges of the square grid circumscribing the collected data and pixels outside the scan region do not accurately depict sample properties. Figure 3c contains zoom-ins of the yellow dashed rectangle. Since all adjacent points are scanned in the same direction the quality for the reconstructed step on the feature is outstanding.

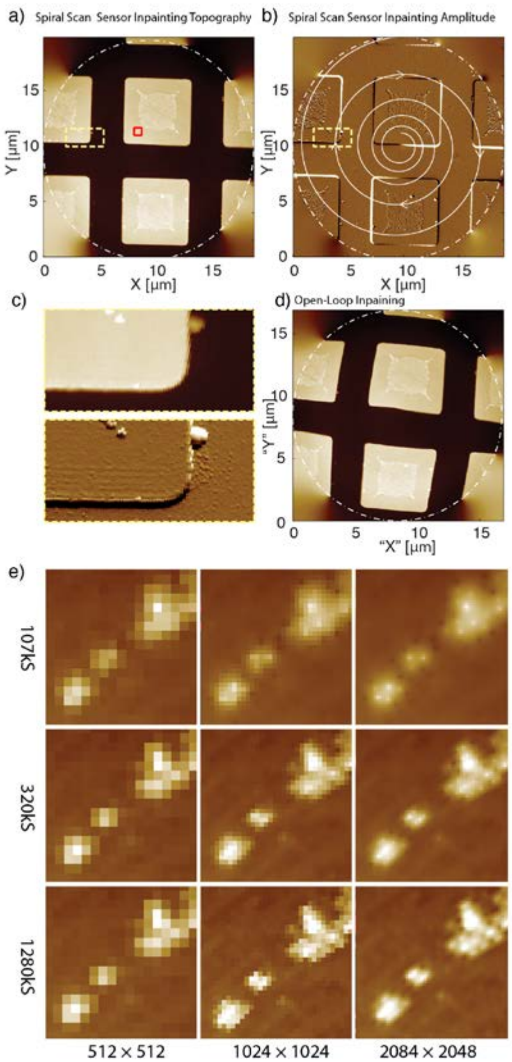

Figure 3. Sensor Inpainting of topography(a) and amplitude(b) data from an Archimedean spiral scan of the calibration sample. 256 loops within an area approximately equal to figure 2f inpainted to a 1024x1024 grid. Image values outside the circle result from the inpainting algorithm diffusing information to the edges where no data was acquired. c) Topography zoom-in of dashed square shows a straight edge, resulting from all adjacent scan segments having the same direction of motion as evidenced by amplitude data. d) Inpainting from position values calculated from scanner drive voltage and first order piezo sensitivity. Hysteresis only leads to slight dilation of the center of the image and rotation along the scan direction. e) Zoom-in of red square region in (a) comparing the effect of increasing the number of recorded samples and the number of pixels used to create the inpainted result. The center image with 320k samples inpainted to a 1024x1024 grid best represents the underlying spiral scan data consisting of 256 loops.

The amplitude data further confirm the fidelity of the image as each scan segment has similar climbing or descending characteristics without offsets. No artifacts from the physical limitations of the X,Y scanner are evident and 100% of the scan data are displayed. Using sensor data for Sensor Inpainting guarantees accurate image generation but it is important to mention that it is equally possible to perform inpainting algorithms on model based position data instead of measured position data from the sensors. This is analogous to open-loop scanning and applicable to any waveforms. Figure 3d shows the inpainted result when the piezo output voltage scaled by the first order piezo sensitivity is used as the position information to create the image. Using an Archimedean spiral, piezo hysteresis results in slight dilation of the center of the image and a rotation in the scan direction. But still 100% of the scan time is used to create the image increasing temporal resolution by over a factor of two compared to raster scanning.

Another advantage of Sensor Inpainting over raster scanning is that the number of data points used to make an image and the number of pixels in the rendered image are variables that can be modulated to optimize image appearance for a given scan size and data point spacing. The number of loops, scan speed, and scan size are the primary independent variables for a spiral scan. Increasing the sampling rate increases the data density along the scan path and has no negative consequences other than increasing file size and longer computation. Similarly, the number of pixels used to render the image can be increased to find the most aesthetically pleasing result. Significant differences between using grid size of 512, 1024, or 2048 pixels only become visible when zooming onto small features. Figure 3e shows the result of changing the number of data points and pixels on a 560 nm x 560 nm area from figure 3a. Each column shows the result of inpainting the differently sampled spiral scan data to different resolution grids. For each row the number of samples and for each column the number of pixels were varied as indicated. The bottom row was sampled at 6.25 kHz resulting in a six times larger distance between loops than distance between samples along the scan direction. For the middle row sampled at 1.56 kHz this ratio is 1.5 and for the top row sampled at 500 Hz it is 0.5, i.e. two loops are two times closer together than two sequential samples along a loop. The lower left and upper right images are extremes of too many data points per pixel or too many pixels per data point. In the lower left image the extra samples provided no new data and the image looks like the image from four times fewer samples. The upper right image is diffuse with occasional bright or dark spots from using heat equation inpainting. Those spots are the sparse data points and the diffuseness is due to the diffusion of their height information. There are clearly not enough samples to create a meaningful image at that resolution. The diagonal from upper left to lower right has about two pixels per data point. The upper left image is too pixelated and does not contain the information of the lower right images. The lower right image looks sharper or more detailed than the middle image. However, while the number of pixels matches the data points well, the data are grouped along the scan direction with missing data between the loops. What appears as fine details around features is due to discrete loops of the spiral and the data being inpainted to too many pixels. The lower middle image contains the same type of error. For this data set and using heat equation inpainting around 1024 pixels on an edge is best. Interestingly, it is preferable to sample about a factor of two more frequently along the scan direction than between spiral loops and to have about a factor of two more pixels than samples.

5. Conclusions

The raster scan paradigm severely limits scanning probe microscopy by dictating scan patterns and operation that is not well suited for piezoelectric nanopositioners. The results are significant expenditure of engineering effort and still a loss of at least half of the data when making images. Sensor Inpainting breaks the raster scan paradigm by rendering accurate images from position sensor using missing data image processing algorithms and provides a software solution to a challenging hardware problem. Since most instruments of recent design have high-speed position sensors built into the scanner, implementation of Sensor Inpainting is simple. It enables the display of 100% of the scan data and alternate scan waveforms, like Archimedean spirals, that are best suited for the physical characteristics of the scanner. Sensor Inpainting allows choosing the amount of pixels in the generated final image. Sampling data a factor of two higher in the fast scan direction and displaying on a grid with around twice as many pixels as samples produces the best representations of the data.

Acknowledgements

We gratefully acknowledge helpful discussions with Yifei Lou, Nen Huynh, Alex Chen, and Jen-Mei Chang. This work was supported by the National Science Foundation Cyber Enabled Discovery and Innovation under Contract No. 940417. Data collection and instrumentation support funded by Office of Science, Office of Basic Energy Sciences, of the U.S. Department of Energy under Contract No. DE-AC02-05CH11231.

References

[1] G. Binnig, C. F. Quate, and C. Gerber, “Atomic Force Microscope,” *Physical Review Letters*, vol. 56, no. 9, pp. 930+, 1986.

[2] G. Binnig, “Atomic force microscope and method for imaging surfaces with atomic resolution,” *US Patent 4724318*, 1986.

[3] G. Binnig, H. Rohrer, C. Gerber, and E. Weibel, “Surface Studies by Scanning Tunneling Microscopy,” *Physical Review Letters*, vol. 49, no. 1, pp. 57+, 1982.

[4] G. Binnig, H. Rohrer, C. Gerber, and E. Weibel, “7 x 7 Reconstruction on Si(111) Resolved in Real Space,” *Physical Review Letters*, vol. 50, no. 2, pp. 120+, 1983.

[5] V. B. Eilings and J. A. Gurley, “Method of driving a piezoelectric scanner linearly with time,” U.S. Patent 5,051,64629-Nov-1990.

[6] J. E. Griffith, G. L. Miller, and C. A. Green, “A scanning tunneling microscope with a capacitance- based position monitor,” *Journal of Vacuum …*, 1990.

[7] N. Tamer and M. Dahleh, “Feedback control of piezoelectric tube scanners,” *… and Control*, 1994.

[8] G. Schitter and A. Stemmer, “Identification and open-loop tracking control of a piezoelectric tube scanner for high-speed scanning-probe microscopy,” *Control Systems Technology, IEEE Transactions on*, vol. 12, no. 3, pp. 449–454, 2004.

[9] Y. Li and J. Bechhoefer, “Feedforward control of a closed-loop piezoelectric translation stage for atomic force microscope,” *Review of Scientific Instruments*, vol. 78, no. 1, pp. 013702–013702–8, 2007.

[10] K. K. Leang and S. Devasia, “Feedback-Linearized Inverse Feedforward for Creep, Hysteresis, and Vibration Compensation in AFM Piezoactuators,” *IEEE Trans. Contr. Syst. Technol.*, vol. 15, no. 5, pp. 927–935.

[11] M. Bertalmio, G. Sapiro, V. Caselles, and C. Ballester, “Image inpainting,” *Proceedings of the 27th annual conference on Computer graphics and interactive techniques, New York, NY, USA, 2000, pp. 417–424.*

[12] W. Baatz, M. Fornasier, P. Markowich and C.-B. Schönlieb, “Inpainting of Ancient Austrian Frescoes,” *Conf. proc. of Bridges, Leeuwarden 2008,* pp. 150-156, 2008.

[13] A. Elhayek, M. Welk and J. Weickert, “Simultaneous Interpolation and Deconvolution Model for the 3-D Reconstruction of Cell Images,” *LNCS, Pattern Recognition, Conf. proc. of DAGM,* vol. 6835, pp. 316-325, 2011.

[14] M. Bertalmio, A.L. Bertozzi and G. Sapiro, “Navier-Stokes, fluid dynamics, and image and video inpainting,” *CVPR 2001, Proc. IEEE Comp. Soc. Conf.*, vol. 1, no. 1, pp. 355-362, 2001.

[15] T.F. Chan, S.H. Kang and J.H. Shen, “Euler's elastica and curvature based inpaintings,” *SIAM J. App. Math.*, vol. 63, no. 2, pp. 564-592, 2002.

[16] T.F. Chan, J. Shen, “Variational image inpainting,” *Comm. Pure and Appl. Math.*, vol. 58, no. 5, pp. 579-619, 2005.

[17] A. Bertozzi, S. Esedoglu and A.Gillette, “Analysis of a two-scale Cahn-Hilliard model for binary image inpainting,” *Multiscale Model. and Simul.*, vol. 6, no. 3,

pp. 913-936, 2007.

[18] T.F. Chan and J. Shen, “Mathematical Models for Local Nontexture Inpaintings,” *SIAM J. Appl. Math.*, vol. 62, no. 3, pp. 1019-1043, 2002.

[19] P. Getreuer, “Total Variation Inpainting using Split Bregman,” *Image Processing Online 2012, http://dx.doi.org/10.5201/ipol.2012.g-tvi , 2012.*

[20] X. Zhang and T.F. Chan, “Wavelet inpainting by nonlocal total variation,” *Inverse Problems and Imaging*, vol. 4, no. 1, pp. 191-210, 2010.

[21] A. Wong and J. Orchard, “A nonlocal-means approach to exemplar-based inpainting,” *ICIP 2008, IEEE Int. Conf. Image Processing*, pp. 2600-2603, 2008.

[22] G. Gilboa and S.J. Osher, “Nonlocal linear image regularization and supervised segmentation,” *Multiscale Model. and Simul.*, vol. 6, no. 2, pp. 595-630, 2007.

[23] A. Buades, B. Coll and J.M. Morel, “A review of image denoising algorithms with a new one,” *Multiscale Model. and Simul.*, vol. 4, no. 2, pp. 490-530, 2005.

[24] G. Yu, G. Sapiro and S. Mallat, “Solving inverse problems with piecewise linear estimators: from Gaussian mixture models to structured sparsity,” *IEEE Trans. on Image Processing*, vol. 21, no. 5, pp. 2481-2499, 2012.

[25] R. Majchrowski, “The Influence of Spiral Sampling on Surface Topography Parameters - Simulation Analysis,” *Komisja Budowy Maszyn Pan – Oddzial W Poznaniu*, 27, Jan. 2007.

[26] M. Wieczorowski, “Spiral Sampling as a fast way of data acquisition in surface topography,” *International Journal of Machine Tools & Manufacture*, pp. 217–2022, Jun. 2012.

[27] A. G. Kotsopoulos and T. A. Antonakopoulos, “Nanopositioning using the spiral of Archimedes: The probe-based storage case,” *Mechatronics*, vol. 20, no. 2, pp. 273–280, Mar. 2010.

[28] S.-K. Hung, “Spiral Scanning Method for Atomic Force Microscopy,” *J. Nanosci. Nanotech.*, vol. 10, no. 7, pp. 4511–4516, Jul. 2010.

[29] I. Mahmood, “Spiral scanning: An alternative to conventional raster scanning in high-speed scanning probe microscopes,” *American Control Conference …*, 2010.

[30] I. A. Mahmood and S. O. Reza Moheimani, “Fast spiral-scan atomic force microscopy,” *Nanotechnology*, vol. 20, no. 36, p. 365503, Aug. 2009.

[31] Y. K. Yong, S. O. R. Moheimani, and I. R. Petersen, “High-speed cycloid-scan atomic force microscopy,” *Nanotechnology*, vol. 21, no. 36, p. 365503, Aug. 2010.

[32] T. Tuma, J. Lygeros, V. Kartik, A. Sebastian, and A. Pantazi, “High-speed multiresolution scanning probe microscopy based on Lissajous scan trajectories,” *Nanotechnology*, vol. 23, no. 18, p. 185501, Apr. 2012.

[33] W. Hua, “Compressed Scan Systems,” *US Patent Application, US2010/0269231A1*, pp. 1–27, Jul. 2011.